AKTA KIMIA
INDONESIA

*Akta Kimindo Vol. 9(2), 2024: 114-132*

# Green Synthesis of $Fe_3O_4$ Nanoparticles Using Pineapple Peel Extract For Adsorption of Rhodamine B

Wahyu Kodarta[1], July F. Sinaga[1], Reza H. Pane[1], Martali U. Pasaribu[1], Ahmad F. Ichasan[1], dan Restina Bemis[1]*

[1]*Chemistry Study Program, Faculty of Science and Technology, Universitas Jambi, UNJA. UNJA Mendalo Campus, Muaro Jambi, Indonesia 36361*

**alamat email korespondensi:restina@unja.ac.id*

**Abstract**

*This research aims to develop an environmentally friendly method for the synthesis of $Fe_3O_4$ nanoparticles using Tangkit pineapple peel extract with iron sand from the Batanghari River, Jambi, as raw materials. FTIR analysis detected Fe-O metal oxide clusters at a wavenumber of 533 $cm^{-1}$, confirming the presence of $Fe_3O_4$. The XRD diffraction pattern according to ICSD reference data number 01-076-0956 shows the highest intensity peak at an angle of 2θ 30.17°; 35.47°; 57.18°; and 62.77° with an average crystal diameter of 19.99 nm. SEM showed irregular particle morphology, while particle size analysis revealed an average particle size of 198 nm. Magnetic properties test using VSM shows that the nanoparticles are superparamagnetic with a saturation magnetization (Ms) of 26.25 emu/g. In the Rhodamine B adsorption test, the highest efficiency was achieved at a mass of 100 mg with a value of 95.21%. The optimum adsorption time occurred at 75 minutes with an efficiency of 98.52%. These results indicate that $Fe_3O_4$ nanoparticles synthesized via the green synthesis method using Tangkit pineapple peel extract have high potential for application in processing textile dye waste.*

***Keyword:*** *green synthesis, $Fe_3O_4$ nanoparticles, bioreductor, environmentally friendly. adsorbent.*

**Abstrak**

*Penelitian ini bertujuan mengembangkan metode ramah lingkungan untuk sintesis nanopartikel $Fe_3O_4$ menggunakan ekstrak kulit nanas Tangkit dengan pasir besi Sungai Batanghari, Jambi, sebagai bahan baku. Analisis FTIR mendeteksi gugus logam oksida Fe-O pada bilangan gelombang 533 $cm^{-1}$, mengonfirmasi keberadaan $Fe_3O_4$. Pola difraksi XRD sesuai data referensi ICSD nomor 01-076-0956 menunjukkan puncak intensitas tertinggi pada sudut 2θ 30,17°; 35,47°; 57,18°; dan 62,77° dengan diameter kristal rata-rata kristal sebesar 19,99 nm. SEM menunjukkan morfologi partikel tidak beraturan,*

*sedangkan analisis ukuran partikel mengungkapkan rata-rata ukuran partikel 141,83 nm. Uji sifat magnetik menggunakan VSM menunjukkan nanopartikel bersifat superparamagnetik dengan magnetisasi saturasi (Ms) sebesar 26,25 emu/g. Pada uji adsorpsi Rhodamin B, efisiensi tertinggi tercapai pada massa 100 mg dengan nilai 95,21%. Waktu adsorpsi optimum terjadi pada 75 menit dengan efisiensi sebesar 98,52%. Hasil ini menunjukkan bahwa nanopartikel $Fe_3O_4$ yang disintesis melalui metode green synthesis menggunakan ekstrak kulit nanas Tangkit berpotensi tinggi untuk aplikasi dalam pengolahan limbah pewarna tekstil.*

***Kata Kunci**: green synthesis, nanopartikel $Fe_3O_4$, bioreduktor, ramah lingkungan, adsorben.*

## I. INTRODUCTION

The Batanghari Watershed (DAS) in Jambi Province is the second largest watershed in Indonesia, with a catchment area of approximately 4.5 million hectares [1], covering most of Jambi Province and parts of West Sumatra Province. The Batanghari River stretches for about 800 kilometers, originating in Jorong Batanghari, Negeri Alahan Panjang, Lembah Gumanti District, Solok Regency. The major tributaries of the Batanghari River include Batang Asai, Batang Tembesi, Batang Merangin, Batang Tabir, Batang Tebo, Batang Bungo, and Batang Suliti. The vast area of the Batanghari Watershed also indicates a potential for substantial iron sand mineral deposits.

Iron sand is a type of sand with a significant concentration of iron, typically dark gray or black in color [2]. Based on initial data obtained by the team through X-Ray Fluorescence (XRF) testing, Jambi sand was found to contain Fe (74.109%), Si (9.124%), Ti (7.826%), Al (3.186%), along with several other elements. The high Fe content makes Jambi's iron sand a potential raw material for the synthesis of $Fe_3O_4$ nanoparticles [3]. $Fe_3O_4$ nanoparticles are utilized as metal adsorbents [4], and drug delivery agents [5].

Previous research has reported that $Fe_3O_4$ nanoparticles can be synthesized using several methods, including the hydrothermal method [6], sol-gel [7], solid-state [8], co-precipitation [9], and other conventional methods. However, these methods generally have several drawbacks, such as difficulties in controlling synthesis parameters like temperature, time, pH, and reagent concentration, all of which can affect the synthesis outcome. Additionally, these methods often require high costs due to the use

of specialized chemicals that are hazardous to both humans and the environment.

To address the weaknesses of these methods, it is necessary to develop environmentally friendly methods, such as green synthesis. The use of natural materials in the green synthesis process is believed to reduce pollutants and pose no health risks. Several plants have been used in the green synthesis of Fe3O4 nanoparticles, including Zanthoxylum armatum leaf extract [10], Imperata cylindrica L. [11], pineapple leaves [12], and Mimba Leaves [13], which both contain phenolic compounds, flavonoids, alkaloids, saponins, and polysaccharides, which have also been used successfully. The novelty of this research is that Tangkit pineapple peel is used which is thought to also contain secondary metabolites such as flavonoids and phenolics so that it can be a natural bioreductor in the formation of 4 nanoparticles. It is known that pineapple production in Tangkit Village reaches ±81.000 fruits per year or around 56.4 tons annually. So far, Tangkit pineapple fruit has only been processed, used in food products such as dodol [14] and other processed foods. However, pineapple skins that have the potential to be processed into high-value products are simply thrown away as waste.

In this research, $Fe_3O_4$ nanoparticles are synthesized through a green synthesis method using pineapple peel extract as a bioreductor to produce an effective adsorbent material for reducing Rhodamine B content in wastewater from the textile dyeing industry. Rhodamine B is a synthetic dye commonly used in the textile, printing, and dyeing industries, classified as a triphenylmethane dye. This dye is widely used in the textile industry and is persistent, difficult to biodegrade, and contains aniline compounds that are toxic, mutagenic, and carcinogenic. The Indonesian Minister of Environment and Forestry issued a regulation (No. P.68/MENLHK/Setjen/Kum.1/8/2016) stipulating that the maximum allowable limit for Rhodamine B in the environment is 5-10 mg/L. If Rhodamine B waste is present in drinking water, it can cause various health issues, such as liver and kidney enlargement, liver function disorders, liver damage, physiological disturbances, and even liver cancer. This dye has been proven to be toxic, capable of causing organ damage in humans, particularly to the liver and kidneys [15].

Although the textile industry has long been a major contributor to environmental pollution, there is still little research being done to effectively address this issue. This innovative research offers a smart solution to tackle the environmental pollution caused by the textile dyeing industry by using $Fe_3O_4$ nanoparticles synthesized in an

environmentally friendly manner with the help of Tangkit pineapple peel extract as a natural bioreductor. The extract aids in the reduction of $Fe^{3+}/Fe^{2+}$ ions into Fe(0) ions during the synthesis of $Fe_3O_4$ nanoparticles, which will later be used as a potential adsorbent for the textile dye Rhodamine B. With its effective dye adsorption capabilities, these nanoparticles present a sustainable alternative for treating textile dye wastewater. Therefore, this research innovation offers new hope for the textile industry to reduce its negative impact on the environment.

## II. METHODOLOGY

This research was conducted from June to October 2023 at the Instrumentation and Final Project Laboratory, Faculty of Science and Technology, Jambi University.

In this study, materials such as iron sand as a source of $Fe_3O_4$, hydrochloric acid (37% HCl), distilled water, pineapple peels, $NH_4OH$, 96% ethanol ($C_2H_5OH$), and distilled water were used. The equipment employed included glassware sets, an oven, a magnetic stirrer, a permanent magnet, a furnace, a Buchner funnel, a rotary evaporator, a reflux apparatus set, a vacuum pump, a 50 mL burette, a water bath, spatulas, stirring rods, sieves, universal indicators, a pH meter, an analytical balance, a heater, porcelain crucibles, a mortar and pestle, filter paper, a vacuum, a centrifuge, a furnace, an autoclave, a sieve shaker, a photocatalytic reactor, Fourier Transformation Infrared (FTIR), X-Ray Fluorescence (XRF), X-Ray Diffraction (XRD), a UV-Vis spectrophotometer, and a vibrating sample magnetometer (VSM).

### 2.1. Preparation of Pineapple Peel Extract

This process follows the procedure outlined by [16]. The collected pineapple peels are washed with water and then dried in an oven at 40°C. The peels are then blended into a fine powder. The obtained pineapple peel powder is placed into a closed container, with 250 grams of powder and 1 liter of 96% ethanol added. The mixture is macerated for 3 × 24 hours. The resulting maceration is then evaporated using a rotary evaporator at 50-60°C. Following this, a phytochemical screening test is conducted. The extract is then used as a bioreductor and capping agent for the synthesis of $Fe_3O_4$.

### 2.2. Green Synthesis of $Fe_3O_4$ NPs

This process follows the procedure outlined by [2], combined with the procedure from [10]. The iron sand is first screened using a sieve shaker 15 times. It is then further screened using an external magnet until dark-colored iron sand is obtained. Forty grams of iron sand are dissolved in 60 mL of 37% HCl (12 M). The mixture is stirred and heated using a magnetic stirrer at 70°C for 60

minutes. The filtrate is then separated from the residue. Subsequently, 5% of the pineapple peel extract is rapidly added to the solution and refluxed for 30 minutes. $NH_4OH$ is then added slowly to the reaction mixture to adjust the pH to 10. A black precipitate is formed and then filtered using an external magnet. The product is washed with distilled water until the pH is neutral. It is then dried in an oven for 2 hours at 100°C. The solid is ground and sieved using a 200-mesh sieve, and then characterized using Fourier Transform Infrared (FTIR) spectroscopy, X-Ray Diffraction (XRD), and a Vibrating Sample Magnetometer (VSM).

### 2.3. Adsorption Testing

**Preparation of Stock Solution**

0.1 gram of Rhodamine B is placed into a 1000 mL volumetric flask and diluted with distilled water to the mark, resulting in a Rhodamine B solution with a concentration of 100 ppm.

**Preparation of Calibration Curve for Rhodamine B Standard Solution**

The 100 ppm Rhodamine B solution is diluted to concentrations of 2, 4, 6, 8, and 10 ppm. Absorbance is measured for the 20 ppm Rhodamine B solution using a UV-Vis spectrophotometer within the wavelength range of 400-800 nm to determine the maximum wavelength (λ max) of Rhodamine B. Absorbance for the Rhodamine B solutions at 2, 4, 6, 8, and 10 ppm is then measured at the obtained λ max using the UV-Vis spectrophotometer. The absorbance values are plotted to create a calibration curve (concentration vs. absorbance).

**Determination of Optimum Mass**

Five 100 mL beakers are each filled with 50 mL of 20 ppm Rhodamine B solution at the optimum pH and are added with synthesized $Fe_3O_4$ powder in amounts of 50, 75, 100, 125, and 150 mg. Stirred with a magnetic stirrer at a constant speed for 60 minutes. The suspension is then filtered, and the absorbance of the filtrate is measured using a UV-Vis spectrophotometer at the maximum wavelength of Rhodamine B.

**Determination of Optimum Time**

Five beakers each measuring 100 mL were filled with 50 mL of 20 ppm Rhodamine B solution and added $Fe_3O_4$ nanoparticles with the optimum mass obtained in the previous procedure. Then stirred with a magnetic stirrer at constant speed for 30, 45, 60, 75, and 150 minutes. The suspension was then filtered and the absorption of the filtrate was measured using a UV-Vis spectrophotometer at the maximum wavelength of Rhodamine B.

### 2.4. Data Analysis

In this study, data analysis includes determining the crystal size of $Fe_3O_4$.

Additionally, statistical analysis is performed to evaluate the optimum adsorption capacity of 4 nanoparticles for Rhodamine B.

**Calculation of Average Crystal Diameter**

Based on the analysis of the $Fe_3O_4$ diffraction data, the average crystal diameter can be determined using the Debye-Scherrer equation:

$$D = \frac{k\,.\lambda}{\beta\,.cos\,\theta} \quad (1)$$

where D is the average crystal diameter in nanometers, K is the Scherrer constant (typically 0.92), $\lambda$ is the X-ray wavelength in nanometers (e.g., for Cu Kα radiation, $\lambda$=0.154nm), $\beta$ is the full width at half maximum (FWHM) of the diffraction peak in radians, θ is the Bragg angle in radians.

**Calculation of % Adsorption of Rhodamine B**

To calculate the percentage of Rhodamine B adsorption, you can use the following formula based on the absorbance data:

$$Adsorption\ (\%) = \frac{(Co-Ce)}{Co}\ x\ 100 \quad (2)$$

where $C_0$ is the initial concentration of Rhodamine B (before adsorption), $C_e$ is the concentration of Rhodamine B at time ttt (after adsorption).

## III. RESULTS AND DISCUSSION

### 3.1. Preparation of Pineapple Peel Extract

The process of preparing pineapple peel extract was carried out using the maceration method. Maceration is a simple method, relatively easy to perform, and does not require extensive equipment [17]. This process involves the use of ethanol as a solvent to extract compounds that are soluble in the solvent. These metabolite compounds are molecules produced by organisms in response to their environment and often have bioactive or pharmacological potential. Secondary metabolites are non-essential compounds for the organism's growth and are found in varying and unique forms among different species.

**Table 1.** Phytochemical Screening Results of Pineapple Peel Extract

| Secondary Metabolite | **Reagent** | **Result** |
|---|---|---|
| Alkaloids | Mayer/Dregendroff | -/- |
| Flavonoids | Mg, HCl, etanol | + |
| Phenolics | $FeCl_3$ 1% | + |
| Quinones | NaOH 1M | - |
| Saponins | Akuades | + |
| Tannins | $FeCl_3$ 1% | + |
| Terpenoids | $H_2SO_4$ | - |

**Note:** (+) contains secondary metabolite compounds (-) does not contain secondary metabolite compounds

**Table 1** presents the results of the phytochemical screening of pineapple peel extract, highlighting the presence of secondary metabolites such as flavonoids, phenolics, saponins, and tannins, while alkaloids, quinones, and terpenoids were absent. Flavonoids, being the largest group of metabolites, are known for their ability to donate hydrogen atoms to neutralize free radicals, halting the progression of radical chain reactions [17]. This makes them effective bioreductants in the green synthesis of $Fe_3O_4$ nanoparticles, as they reduce $Fe^{3+}/Fe^{2+}$ ions to Fe(0). The successful reduction is marked by a color change from yellow to black, indicating nanoparticle formation. Phenolic compounds, also present in the extract, further enhance the reduction process, while saponins and tannins act as natural capping agents, stabilizing the nanoparticles and preventing agglomeration. This stabilization ensures that the nanoparticles maintain their uniformity and dispersion, critical for their application in environmental remediation. The absence of alkaloids, quinones, and terpenoids suggests that the reduction and stabilization roles in this synthesis are primarily driven by the detected metabolites. Overall, the results confirm the potential of pineapple peel extract as an eco-friendly bioreductant for synthesizing $Fe_3O_4$ nanoparticles, providing a green alternative to conventional methods that rely on harmful chemicals.

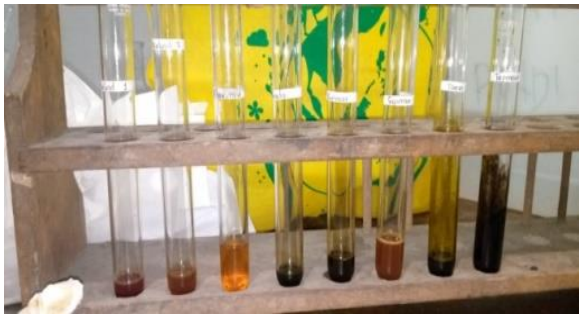

**Figure 1.** Phytochemical Screening Results

### 3.2. Synthesis of $Fe_3O_4$ Nanoparticles

Secondary metabolites present in pineapple peel act as reducing agents in the formation of nanoparticles. One key indicator of magnetic nanoparticle formation during synthesis is the color change from brownish-yellow to deep black. This color change signifies the reduction of $Fe^{3+}/Fe^{2+}$ ions to Fe(0). The reaction mechanism can be observed in Fig 2.

Fig 2. illustrates the mechanism for the formation of $Fe_3O_4$ nanoparticles by utilizing iron sand as a source of Fe ions and flavonoids from pineapple peel as a natural reducing agent. The process begins with the extraction of Fe ions from iron sand using an HCl solution, which produces a solution rich in Fe(II) and Fe(III) ions. These ions then interact with flavonoids through a series of complex redox reactions. The mechanism begins with the interaction of flavonoids with Fe(II) and Fe(III) ions through a redox reaction, where flavonoids are oxidized and

Fe(II) and Fe(III) ions are reduced. In this process, Fe(II) is oxidized to Fe(III), and Fe(III) is reduced to Fe(II). Flavonoids release electrons ($e^-$) and hydrogen ions ($H^+$), resulting in changes to the chemical structure of flavonoids. The reaction continues with Fe(II) and Fe(III) from the first step being reduced to Fe(0) through a redox reaction with flavonoids. Further oxidation of flavonoids produces Fe(0) as a product. Fe(0) then interacts with each other and begins to form $Fe_3O_4$ nanoparticles. These nanoparticles are naturally stabilized during the growth and nucleation processes to ensure uniform and stable sizes. This figure demonstrates how flavonoids act not only as reducing agents converting Fe ions to their metallic form (Fe(0)) but also assist in the formation and stabilization of iron oxide nanoparticles.

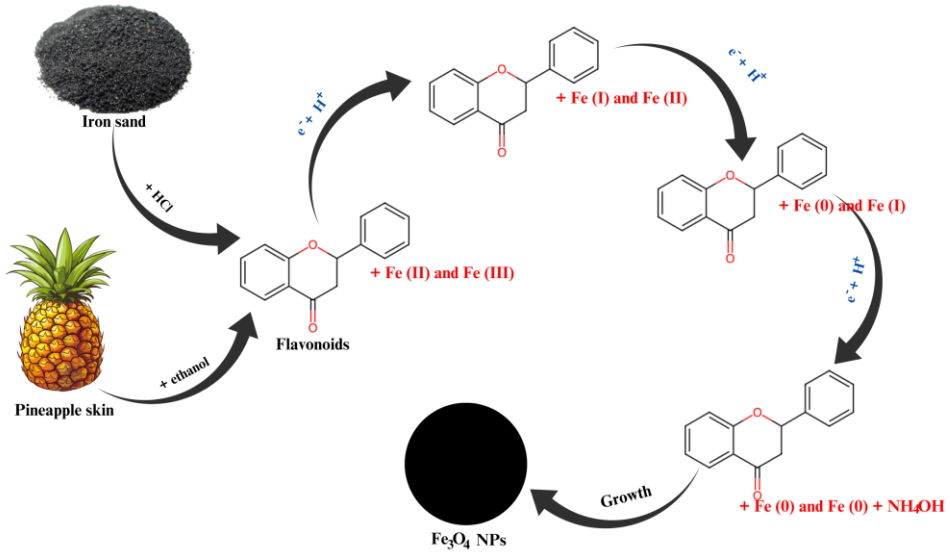


**Figure 2**. Reaction Mechanism for the Formation of $Fe_3O_4$ Nanoparticles

***Fourier Transform Infrared* (FTIR)**

The FTIR characterization results of the $Fe_3O_4$ synthesis demonstrate the successful formation of the material with the identification of several main functional groups, such as Fe-O, C-H, C=C, C=O, and OH. The Fe-O group detected at a wavenumber of 533 $cm^{-1}$ is a characteristic feature of the spinel $Fe_3O_4$ structure, and this result is consistent with previous studies reporting Fe-O detection at 586.36 $cm^{-1}$ [3], 587 $cm^{-1}$ [10], and 547 $cm^{-1}$ [18]. This indicates that the $Fe_3O_4$ synthesis produced the desired material structure. Additionally, the C-H group detected at 1423 $cm^{-1}$ is likely derived from organic molecules adsorbed on the material's surface, possibly from solvents or precursors that did not fully evaporate

during the synthesis process. The C=C group detected at 1606 $cm^{-1}$ suggests the presence of a carbon-carbon double bond, likely from residual organic material involved in the synthesis reaction or adsorbed on the $Fe_3O_4$ surface. The detection of the C=O group at 1981 $cm^{-1}$ indicates the presence of a carbonyl compound, which may have formed as a byproduct or from interactions with the surrounding environment during synthesis.

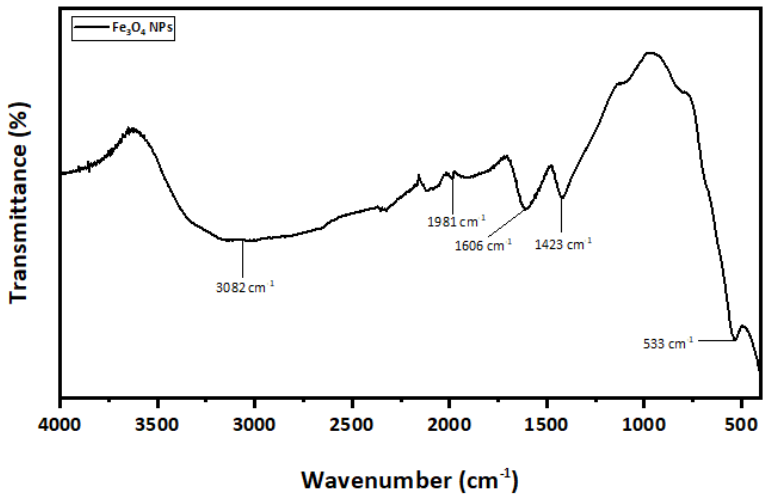


**Figure 3.** FTIR Spectra $Fe_3O_4$ NPs

Meanwhile, the detection of the hydroxyl (OH) group at 3082 $cm^{-1}$ is lower than the values reported in the literature (3417–3448 $cm^{-1}$) [3], [10], [18]. This shift can be explained by strong interactions between the OH group and the $Fe_3O_4$ surface, indicating the formation of hydrogen bonds between the hydroxyl group and the material's surface. Additionally, this shift could also be caused by moisture trapped within the material during the synthesis process or FTIR measurement. The moisture may bind to the OH groups, causing a shift in the wavenumber to a lower value compared to the literature. Inadequate drying conditions could also affect the peak intensity, as discussed by [8].

**Table 2.** Interpretation of FTIR spectrum data

| Sample | Synthesis Results | Wavenumber ($cm^{-1}$) | | |
|---|---|---|---|---|
| | | [3] | [10] | [18] |
| $Fe_3O_4$ | 533 (Fe-O) | 586.36 (Fe-O) | 587 (Fe-O) | 547 (Fe-O) |
| | 1423 (C-H) | - | 1441 (C-H) | 1406 (C-H) |
| | 1606 (C=C) | - | 1631(C=C) | 1614 (C=C) |
| | 1981 (C=O) | - | - | - |
| | 3082 (OH) | 3448.72 (OH) | 3417 (OH) | 3425 (OH) |

***X-Ray Diffraction* (XRD)**

XRD characterization was performed to identify the crystal structure, crystallinity, and crystal size of the sample. The analysis was conducted using an X-ray tube with Cu radiation (1.54060 Å), operating at 40 kV and 30.0 mA. The obtained diffraction data were processed using the Debye-Scherrer formula. The diffractogram was further analyzed by comparing the diffraction patterns with standard patterns from the International Centre for Diffraction Data (ICSD). The XRD diffractogram for the $Fe_3O_4$ sample is presented in Fig 4.

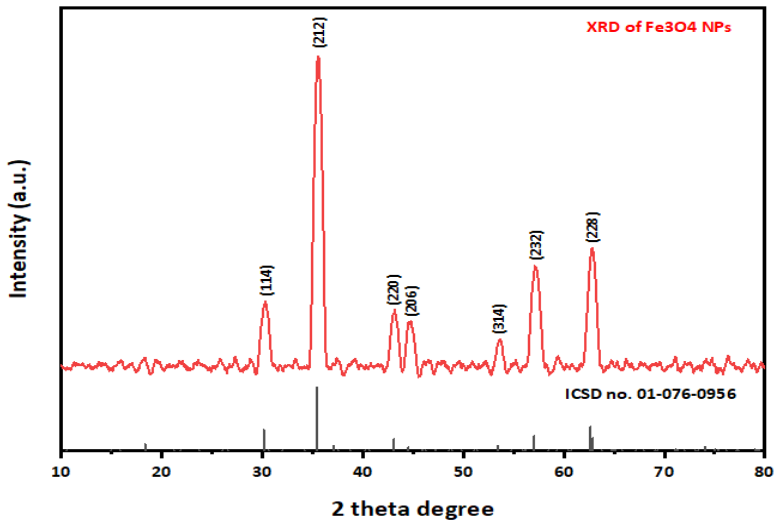


**Figure 4.** XRD Diffractogram of Synthesized $Fe_3O_4$

The X-ray Diffraction (XRD) characterization results of the synthesized $Fe_3O_4$, as shown in Fig 4, reveal several significant diffraction peaks indicating the formation of a crystalline structure. The main peaks are detected at 2θ angles of 30.17°, 35.47°, 57.18°, and 62.77°, corresponding to the crystal planes (114), (212), (232), and (228). Additionally, lower intensity peaks are observed at 2θ angles of 43.27°, 44.42°, and 53.47°, associated with the crystal planes (220), (206), and (314).

These XRD results closely match the reference data from the International Centre for Diffraction Data (ICSD) number 01-076-0956, indicating a very good alignment with the diffraction peaks of the synthesized $Fe_3O_4$ sample. The similarity in peak positions confirms that the $Fe_3O_4$ formed has a crystal structure consistent with the inverse spinel cubic phase, suggesting that the synthesis process was effective and produced a product in agreement with the reference data. Previous studies [19] showed diffraction peaks at nearly

identical angles, with high-intensity peaks at 2θ angles of 30.2°, 35.6°, 53.7°, and 62.9°.

The sharp and intense peaks in the XRD pattern indicate that the $Fe_3O_4$ crystals formed have high quality, with an average crystal diameter of 19.99 nm. This small crystal size is crucial as it provides unique material properties, such as increased surface area and faster response in various applications. The crystallinity degree of the produced $Fe_3O_4$ is measured at 60.09%, indicating that most of the material has an orderly crystal structure with minimal amorphous phase. This high degree of crystallinity suggests that the produced $Fe_3O_4$ possesses excellent physical and chemical properties, which are essential for optimal performance in technological applications.

**Scanning Electron Microscope (SEM)**

The results of morphological analysis using Scanning Electron Microscopy (SEM) show the visual characteristics of $Fe_3O_4$ particles which have irregular size and distribution, and agglomeration occurs. Particle size analysis showed that the average particle size was *141,83 nm*. In images with magnifications of 5000 and 9000x, small micron-sized particles can be seen starting to combine to form aggregations.

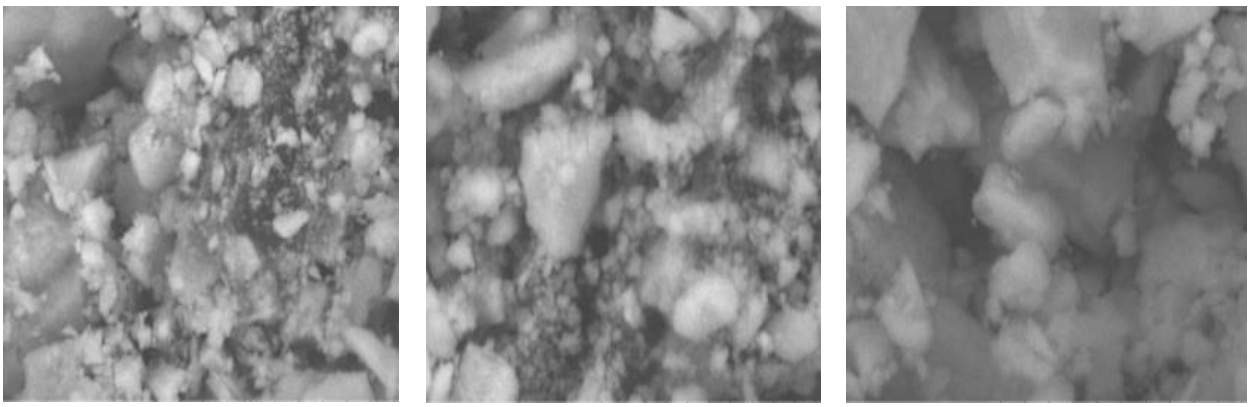

(a) (b) (c)

**Figure 5.** SEM analysis results (a) 5000x (b) 9000x and (c) 10,000x

The distribution of particles that appears to vary indicates that the synthesis process has not been able to produce uniform particle sizes. This variation can occur because synthesis conditions such as precursor concentration, temperature, and reaction time are not completely optimal. In images with 10,000x magnification, agglomeration is more dominant, with small particles interacting with each other to form dense structures. The high magnetic attraction between $Fe_3O_4$ particles is the main factor that drives these particles to

stick together. This is a common phenomenon in magnetic materials, where local magnetic fields generated by individual particles create strong attractive interactions [20].

According to [21], a reaction temperature that is too high can accelerate crystal growth, thereby increasing particle size and triggering cluster formation. Likewise, a reaction time that is too long can cause the particles to continue to enlarge and interact with each other until they form large aggregations. In addition, nucleation can affect the uniformity of $Fe_3O_4$ crystals during synthesis. High temperature particle distribution can cause uncontrolled crystal growth. This phenomenon, known as Ostwald Ripening, occurs when smaller particles become smaller and larger particles become larger

**Vibrating Sample Magnetometer (VSM)**

Based on Table 3 and Fig 6, the magnetic properties of $Fe_3O_4$ nanoparticles were measured using a Vibrating Sample Magnetometer (VSM), resulting in a hysteresis curve that reveals three main magnetic parameters: saturation magnetization (Ms), magnetic remanence (Mr), and coercivity (Hc). The recorded saturation magnetization (Ms) value of 26.25 emu/g indicates the maximum capacity of $Fe_3O_4$ nanoparticles to generate magnetic moments when a strong external magnetic field is applied. This value is lower compared to the study by [10], which obtained an Ms value of 143 emu/g. This difference is likely due to the difference in raw materials used; [10] used a Fe solution as the iron source for $Fe_3O_4$ synthesis, while this study used iron sand as the Fe source. Iron sand, with its lower purity and potential impurities, may contribute to the reduced Ms value compared to using a purer Fe solution. The magnetic remanence (Mr) value obtained was 1.048, indicating the residual magnetization in the material after the external field is removed. This low Mr value suggests superparamagnetic characteristics, where the magnetic moments of nanoparticles quickly return to a non-magnetic state once the external field is removed. This is also supported by the relatively low coercivity (Hc) value of 1.48, indicating that the material requires a small magnetic field to eliminate residual magnetization. This magnetic behavior reflects that the $Fe_3O_4$ nanoparticles produced in this study have characteristics suitable for applications in magnetic systems requiring quick responses, such as in biomedical technologies or magnetic catalysis. Despite the lower Ms value compared to the study by [10], using iron sand as a raw material could be a more cost-effective and environmentally friendly alternative.

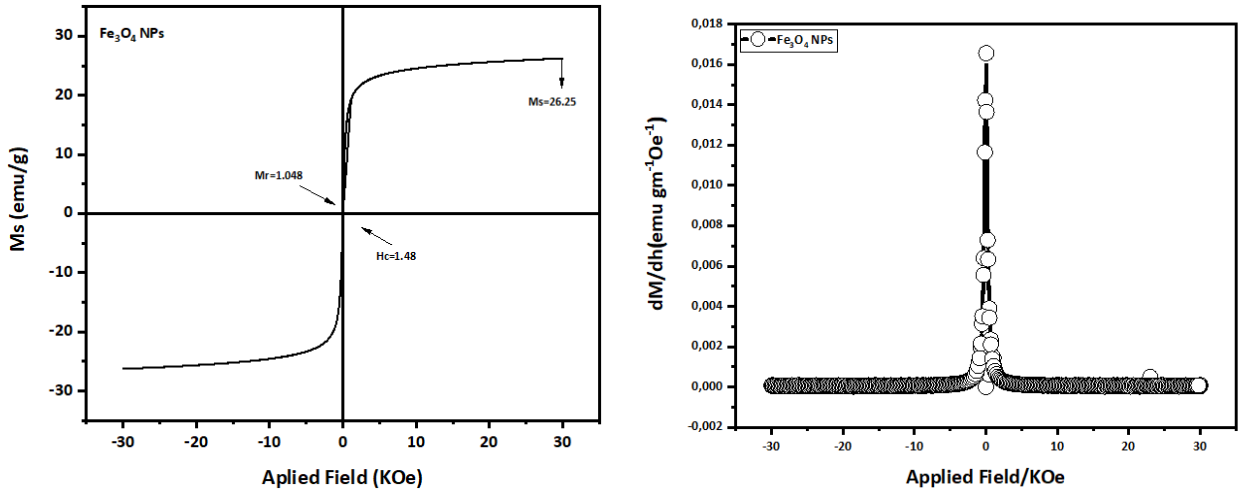


**Figure 6.** Hysteresis curve of $Fe_3O_4$ Nanoparticles (a) and Magnetic moment differential curve (b)

**Table 3.** Magnetic Properties Parameters

| Sample | Ms (emu/g) | Mr | Hc |
|---|---|---|---|
| $Fe_3O_4$ | 26.25 | 1.048 | 1.48 |

**Note:** Ms = Saturation Magnetization, Mr = Remanence, Hc = Coercivity.

The curve from the VSM measurement of $Fe_3O_4$ nanoparticles shows typical superparamagnetic characteristics. In the applied magnetic field (H), the differential magnetic moment curve (dM/dH) exhibits a sharp peak around zero field (0 KOe), with a maximum value reaching 0.0017 emu/gOe. This reflects a significant magnetic response at low fields, where magnetic particles spontaneously magnetize without a strong external field. The sharp decrease in dM/dH as the magnetic field moves away from zero, in both positive and negative directions, indicates a rapid transition to magnetic saturation. At ±10 KOe, the dM/dH value decreases to 0.0005 emu/gOe and continues to flatten until it nearly reaches zero at ±20 KOe, indicating that further increases in the magnetic field do not cause significant increases in magnetic moment. This suggests that at high fields, $Fe_3O_4$ nanoparticles reach magnetic saturation, where all magnetic moments in the material align with the applied field. The observed superparamagnetic behavior in $Fe_3O_4$ nanoparticles is due to their very small size, which makes thermal energy strong enough to change the direction of

magnetic moments within the nanoparticles. In this state, the material does not exhibit significant magnetic hysteresis, as evidenced by the absence of a characteristic magnetization loop for ferromagnetic materials. This behavior indicates that $Fe_3O_4$ nanoparticles have potential for various applications in technologies such as magnetic data storage, magnetic hyperthermia, and contrast agents in magnetic resonance imaging (MRI).

### 3.3. Adsorption Study

In this research, $Fe_3O_4$ nanoparticles were used as adsorbents to remove Rhodamine B dye from the solution. Adsorption analysis was carried out by looking at the effect of Rhodamine B concentration on absorption and the effect of adsorbent mass on the adsorption percentage. Apart from that, the interaction mechanism between adsorbate and adsorbent was also studied.

The first step taken was to create a calibration curve, namely the curve. The relationship between Rhodamine B concentration and absorbance was measured using UV-Vis spectrophotometry. Based on the data obtained, a linear relationship was found between the concentration of the solution and the absorption value at a certain wavelength, as shown in Fig 7.

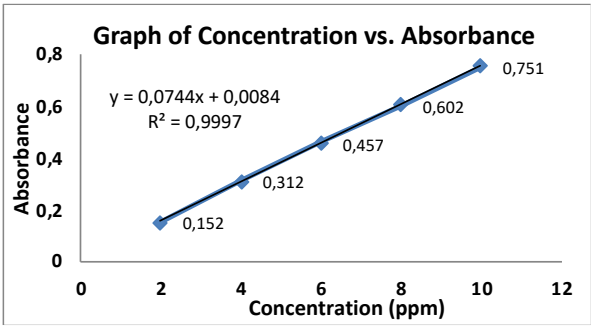


**Figure 7.** Graph of Concentration vs. Absorbance

Fig 7 shows an excellent correlation between concentration and absorbance, with the linear regression equation given by y = 0.0744x + 0.0084 and an $R^2$ value of 0.9997. This high coefficient of determination indicates that the regression equation can accurately estimate the concentration of Rhodamine B in solution based on the measured absorbance values. The adherence to Beer's Law, which states that absorbance is directly proportional to the concentration of the solution, further supports the reliability of UV-Vis spectrophotometry in measuring Rhodamine B concentration under these experimental conditions.

Next, an evaluation was carried out on the effect of $Fe_3O_4$ adsorbent mass and contact time on Rhodamine B adsorption efficiency, as well as analyzing the chemical interactions that occurred during the adsorption process. Variations in the mass of the $Fe_3O_4$ adsorbent were carried out to determine the optimum

adsorbent mass for Rhodamine B adsorption efficiency. The relationship between adsorbent mass and Rhodamine B adsorption percentage is shown in Fig 8.

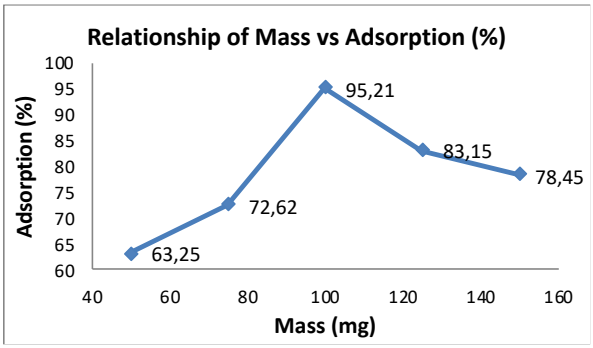


**Figure 8.** Graph of the relationship between Mass vs. % Adsorption

In Fig 8, it can be seen that the adsorption percentage increases with increasing adsorbent mass until it reaches a maximum value of 95.21% at an adsorbent mass of 100 mg. This is in line with the statement [22] that increasing the adsorbent mass can increase the number of active sites on the $Fe_3O_4$ surface. This active site allows more Rhodamine B molecules to be adsorbed through chemical interactions, such as electrostatic interactions and hydrogen bond formation. The hydroxyl group (-OH) on the $Fe_3O_4$ surface experiences deprotonation, producing a negative charge which plays a role in the adsorption process which can be seen in reaction equation (3).

$$Fe_3O_4(\text{-OH}) \rightleftharpoons Fe_3O_4(\text{-O}^-) + H^+ \quad (3)$$

This deprotonation generates a negative charge on the $Fe_3O_4$ surface, facilitating electrostatic interactions with the positively charged RhB:

$$RhB^+ + Fe_3O_4(\text{-O}^-) \rightarrow RhB\text{-}Fe_3O_4 \quad (4)$$

Additionally, the hydroxyl groups on $Fe_3O_4$ can form hydrogen bonds with the carbonyl (-C=O) or amino ($-NH_2$) groups of RhB:

$$Fe_3O_4(\text{-OH}) + RhB \rightarrow Fe_3O_4\cdots H{-}RhB \quad (5)$$

However, after reaching an adsorbent mass of 100 mg, further increasing the adsorbent mass actually caused a decrease in adsorption efficiency to 78.45% at a mass of 150 mg. This phenomenon is caused by the saturation effect, where the number of Rhodamine B molecules in solution becomes limited compared to the number of active sites available. As a result, some of the active sites on the $Fe_3O_4$ surface remain unused, thus providing no additional contribution to the adsorption enhancement.

Next, the optimum contact time was determined where the adsorbent mass used was the optimum mass obtained from previous results, namely 100 mg. The relationship between time and the percentage of Rhodamine B adsorption is shown in Fig 9.

Fig 9 shows the relationship between variations in contact time and adsorption percentage, which reflects the efficiency of the adsorption process over time. Based on the data in the graph, it can be seen that at 30

minutes the adsorption percentage was recorded at 91.68%. At this initial stage, the adsorbate molecules begin to interact with the adsorbent surface but have not yet reached optimal conditions. As time goes by, the adsorption percentage increases until it reaches 92.13% at 45 minutes and 95.21% at 60 minutes, this shows that more and more adsorbate molecules are successfully attached to the available adsorbent surface.

The adsorption peak was achieved at 75 minutes with a maximum percentage of 98.52%, indicating the optimal contact time for the adsorption process. At this point, nearly all active adsorbent surfaces were saturated with adsorbate molecules. However, after 75 minutes, a decrease in adsorption percentage was observed, dropping to 93.15% at 90 minutes. This decrease was likely caused by the saturation of the adsorbent surface, reducing its capacity to retain additional molecules. Furthermore, desorption or the release of adsorbate molecules from the adsorbent surface could also contribute to the decline.

These findings align with previous studies that demonstrated the significant influence of contact time on adsorption efficiency. For instance, research by [22] found that increasing initial contact time resulted in a significant rise in adsorption until reaching an optimal time, after which a decrease occurred due to adsorbent saturation. Another study by [23] revealed a similar pattern, where maximum adsorption was achieved at a specific contact time, followed by a decline in efficiency due to adsorbate desorption.

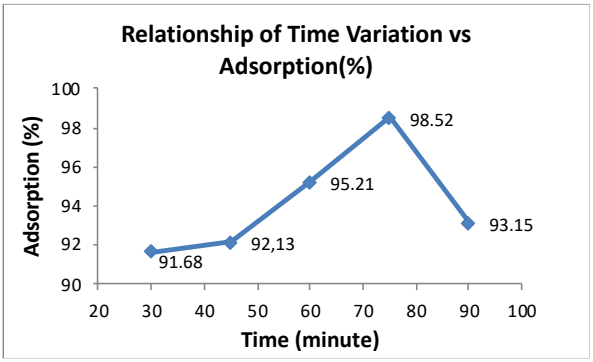


**Figure 9.** Graph of the Relationship of Time Variation vs Adsorption(%)

## IV. CONCLUSION

The synthesis of $Fe_3O_4$ nanoparticles was successfully achieved using a green synthesis method with pineapple peel extract as the bioreductor, containing secondary metabolites such as flavonoids, tannins, and saponins. The synthesized nanoparticles were characterized using XRD, FTIR, SEM, and VSM. XRD confirmed that the nanoparticles have a crystal structure consistent with magnetite diffraction patterns. FTIR identified Fe-O groups and interactions with compounds from the pineapple peel extract. SEM revealed uniform nanometer-sized particles, and VSM demonstrated good magnetic properties with

saturation magnetization close to ideal values. Additionally, the $Fe_3O_4$ nanoparticles exhibited high adsorption efficiency was achieved at a mass of 100 mg with a value of 95.21%. The optimum adsorption time occurred at 75 minutes with an efficiency of 98.52%. highlighting their potential for industrial waste treatment applications. This green synthesis method proves to be environmentally friendly and sustainable compared to conventional chemical methods.

## ACKNOWLEDMENTS

We would like to express our gratitude to the Ministry of Education, Culture, Research, and Technology (Kemendikbudristek) for funding our research through the 2023 Student Creativity Program (PKM). We also extend our thanks to Jambi University for providing full support for this research activity, as well as to the Final Project Laboratory, Faculty of Science and Technology, Jambi University for facilitating our study. The support from all parties has been instrumental in the smooth execution and success of this research.

## REFERENCES

[1] S. H. Putri, "Daerah Aliran Sungai (DAS) Batanghari: Rupa Bumi Nan Kaya Sejarah," vol. 4, no. 1, pp. 21–31, 2024.

[2] O. Elsafitri and F. Deswardani, "Sintesis Dan Karakterisasi Nanopartikel $Fe_3O_4$ (Magnetite) Dari Pasir Besi Sungai Batanghari Jambi Yang Dienkapsulasi Dengan Polyethylene Glycol (Peg-4000)," *J. Pendidik. Fis. Tadulako*, vol. 8, no. 3, pp. 97–103, 2020.

[3] Heriansyah, Mustawarman, and E. Suharyadi, "($Fe_3O_4$) YANG DIENKAPSULASI POLIMER POLYETHYLENE GLYCOL ( PEG-4000 )," *Spektra J. Fis. dan Apl.*, vol. 16, no. 3, pp. 50–55, 2015.

[4] G. D. Tatinting and H. F. Aritonang, "DARI PASIR BESI PANTAI HAIS SEBAGAI ADSORBEN LOGAM KADMIUM ( Cd )," vol. 14, no. 2, 2021.

[5] D. Indiastuti and F. F. Amaliyah, "SintesisIndiastuti, Dian, and Fina Firatun Amaliyah. 2021. 'Sintesis Dan Karakterisasi Nanopartikel $Fe_3O_4$ Termodifikasi Biokompatibel Polimer Serta Potensinya Sebagai Penghantar Obat.' The Indonesian Green Technology Journal: 1–8. dan Karakterisasi Nanopa," *Indones. Green Technol. J.*, pp. 1–8, 2021, doi: 10.21776/ub.igtj.2021.010.01.01.

[6] D. Novita and A. Astuti, "Sintesis dan Karakterisasi Sifat Optik Nanokomposit $Fe_3O_4$@CQD (Carbon Quantum Dots),"

*J. Fis. Unand*, vol. 12, no. 2, pp. 310–315, 2023, doi: 10.25077/jfu.12.2.310-315.2023.

[7] S. Widodo, "Teknologi Pembuatan Magnetite Nanopartikel Dengan Metode Sol-Gel Untuk Lapisan Aktif Sensor Gas," *Techno-Socio Ekon.*, vol. 15, no. 2, pp. 98–105, 2022, doi: 10.32897/techno.2022.15.2.1216.

[8] S. Taib and E. Suharyadi, "Sintesis Nanopartikel Magnetite ($Fe_3O_4$) dengan Template silika ($SiO_2$) dan Karakterisasi Sifat Kemagnetannya," *Indones. J. Appl. Phys.*, vol. 5, no. 01, p. 23, 2015, doi: 10.13057/ijap.v5i01.256.

[9] S. Husain *et al.*, "Potensi Nanokomposit $Fe_3O_4$@C dari Bijih Besi Sebagai Pendeteksi Kadar Glukosa," *Positron*, vol. 9, no. 2, p. 44, 2019, doi: 10.26418/positron.v9i2.32771.

[10] A. V. Ramesh, D. Rama Devi, S. Mohan Botsa, and K. Basavaiah, "Facile green synthesis of $Fe_3O_4$ nanoparticles using aqueous leaf extract of Zanthoxylum armatum DC. for efficient adsorption of methylene blue," *J. Asian Ceram. Soc.*, vol. 6, no. 2, pp. 145–155, 2018, doi: 10.1080/21870764.2018.1459335.

[11] A. Siti Zulaicha, I. Syahjoko Saputra, I. Puspita Sari, and D. Annas, "Sintesis dan Kararkterisasi Modifikasi Mikropartikel Magnetit ($Fe_3O_4$) Dalam Pemanfaatan Karat dengan Ekstrak Daun Ilalang (Imperata Cylindrica L)," *J. Jejaring Mat. dan Sains*, vol. 2, no. 2, pp. 51–55, 2020, doi: 10.36873/jjms.2020.v2.i2.405.

[12] A. W. Y. Putra Parmita *et al.*, "Studi Pengaruh Temperatur Kalsinasi dalam Pembentukan Nanomagnetite dengan Metode Green Synthesis Ekstrak Daun Nanas," *SPECTA J. Technol.*, vol. 7, no. 2, pp. 584–592, 2023, doi: 10.35718/specta.v7i2.940.

[13] M. Syihabuddin, "GREEN SYNTHESIS NANOPARTIKEL $Fe_3O_4$ DENGAN BIOREDUKTOR EKSTRAK DAUN MIMBA (Azadirachta indica) : APLIKASI SEBAGAI MATERIAL FOTOKATALIS DEGRADASI METHYLENE BLUE," vol. 13, pp. 118–123, 2024.

[14] T. Zulfikar *et al.*, "Branding dan Digital Marketing Meningkatkan Penjualan pada Pelaku Usaha Dodol Nanas Desa Tambakmekar Jalancagak Kabupaten Subang," *J. Abdimas Perad.*, vol. 3, no. 1, pp. 41–47, 2022, doi: 10.54783/ap.v3i1.7.

[15] S. Gul *et al.*, "Enhanced Adsorption of Rhodamine B on Biomass of Cypress/False Cypress (Chamaecyparis lawsoniana) Fruit: Optimization and

Kinetic Study," *Water (Switzerland)*, vol. 14, no. 19, 2022, doi: 10.3390/w14192987.

[16] V. Damogalad, H. Jaya Edy, and H. Sri Supriati, "Formulasi Krim Tabir Surya Ekstrak Kulit Nanas (Ananas Comosus L Merr) Dan Uji in Vitro Nilai Sun Protecting Factor (Spf)," *PHARMACON J. Ilm. Farm. – UNSRAT*, vol. 2, no. 02, pp. 2302–2493, 2013.

[17] R. Bemis, F. Deswardani, H. Heriyanti, R. D. Puspitasari, and N. Azizah, "Green Synthesis of Silver Nanoparticles Using Areca Catechu L Peel Bioreductor as an Antibacterial Escherichia Coli and Staphylococcus Aureus," *IJCA (Indonesian J. Chem. Anal.*, vol. 6, no. 2, pp. 176–186, 2023, doi: 10.20885/ijca.vol6.iss2.art9.

[18] G. M. Sulaiman, A. T. Tawfeeq, and A. S. Naji, "Biosynthesis, characterization of magnetic iron oxide nanoparticles and evaluations of the cytotoxicity and DNA damage of human breast carcinoma cell lines," *Artif. Cells, Nanomedicine Biotechnol.*, vol. 46, no. 6, pp. 1215–1229, 2018, doi: 10.1080/21691401.2017.1366335.

[19] N. R. Jannah and D. Onggo, "Synthesis of $Fe_3O_4$ nanoparticles for colour removal of printing ink solution," *J. Phys. Conf. Ser.*, vol. 1245, no. 1, 2019, doi: 10.1088/1742-6596/1245/1/012040.

[20] G. Wang, H. Zhang, and X. Liu, "Magnetic Interaction and Agglomeration Behavior of Iron Oxide Nanoparticles: An Insight into Morphological Influence," *Journal of Magnetic Materials*, vol. 427, no. 2, pp. 259-267, 2017.

[21] X. Li, Y. Zhao, and Q. Chen, "Effect of Reaction Temperature on the Crystalline Growth and Morphology of Magnetic Nanoparticles," *Materials Chemistry and Physics*, vol. 230, no. 5, pp. 122-130, 2019.

[22] J. Smith, T. Brown, and P. Johnson, "Effect of Contact Time on Adsorption Efficiency Using Activated Carbon as an Adsorbent," *Journal of Environmental Chemistry*, vol. 45, no. 3, pp. 123-130, 2020.

[23] R. Kumar, A. Singh, and P. Gupta, "Optimization of Adsorption Parameters for Dye Removal: The Role of Contact Time, Adsorbent Dose, and pH," *International Journal of Chemical Engineering*, vol. 36, no. 4, pp. 245-253, 2019..